Journal of Rock Mechanics and Geotechnical Engineering xxx (xxxx) xxx

Contents lists available at ScienceDirect

Journal of Rock Mechanics and Geotechnical Engineering

journal homepage: www.jrmge.cn

Full Length Article

# An unsupervised incremental learning model to predict geological conditions for earth pressure balance shield tunneling

Jiajie Zhen [a], Fengwen Lai [a], Jim S. Shiau [b], Ming Huang [a,*], Yao Lu [a], Jinhua Lin [c]

[a] College of Civil Engineering, Fuzhou University, Fuzhou, 350108, China
[b] School of Engineering, University of Southern Queensland, Toowoomba, QLD, 4350, Australia
[c] China Communications Construction First Highway Engineering Bureau Xiamen Co., Ltd., Xiamen, 361021, China

ARTICLE INFO

*Article history:*
Received 26 August 2024
Received in revised form
24 December 2024
Accepted 30 December 2024
Available online xxx

*Keywords:*
Deep temporal clustering
Geological condition perception
Incremental learning
Shield tunnel

ABSTRACT

Current machine learning models for predicting geological conditions during earth pressure balance (EPB) shield tunneling predominantly rely on accurate geological conditions as model label inputs. This study introduces an innovative approach for the real-time prediction of geological conditions in EPB shield tunneling by utilizing an unsupervised incremental learning model that integrates deep temporal clustering (DTC) with elastic weight consolidation (EWC). The model was trained and tested using data from an EPB shield tunneling project in Nanjing, China. Results demonstrate that the DTC model outperforms nine comparison models by clustering the entire dataset into four distinct groups representing various geological conditions without requiring labeled data. Additionally, integrating EWC into the DTC model significantly enhances its continuous learning capabilities, enabling automatic parameter updates with incoming data and facilitating the real-time recognition of geological conditions. Feature importance was evaluated using the feature elimination method and the Shapley additive explanations (SHAP) method, underscoring the critical roles of earth chamber pressure and cutterhead rotation speed in predicting geological conditions. The proposed EWC-DTC model demonstrates practical utility for EPB shield tunneling in complex environments.


## 1. Introduction

The earth pressure balance (EPB) machine has been widely employed in metro tunnel construction due to its advantages of automation, high-efficiency, and safe construction practices (Cheng et al., 2021; Huang et al., 2023; Yan et al., 2023; Lu et al., 2024). It is well established that the timely adjustment of shield operational parameters is crucial because the shield cutterhead is highly sensitive to changing geological conditions (Zhou et al., 2019a; Qian et al., 2021a; Lu et al., 2023; Wang et al., 2023, 2024; Lai et al., 2024; Liu et al., 2024a,b,c). Incorrect parameter adjustments can lead to severe consequences such as tunnel misalignment, damage to machinery, extended construction timelines, and substantial economic losses (Liu et al., 2021, 2024; Chen et al., 2023). Consequently, the ability to accurately and promptly predict the geological conditions during shield tunneling is essential to mitigate these risks and ensure smooth project execution.

The narrow gap between the cutterhead and the tunnel face poses challenges for conventional exploration and in-situ testing methods to effectively obtain surrounding geological condition parameters. Borehole drilling, while an essential exploratory tool, is constrained by the number and spacing of boreholes, which limits the comprehensive understanding of geological formations (Cheng et al., 2021; Yang et al., 2023; Liu et al., 2024a,b,c). Ground penetrating radar (GPR) and tunnel seismic prediction (TSP) methods, which rely on reflected electromagnetic waves, offer valuable insights but are often limited by cost, time requirements, and complexities in data interpretation, particularly in complex geological environments (Li et al., 2017; Zhou et al., 2022; Liu et al., 2023). Therefore, there is a need for a more effective and economical solution that enables the real-time prediction of geological conditions during shield tunneling. Shield tunneling is inherently dynamic and characterized by the complex interactions between the shield tunneling machine and its surrounding geological environment

* Corresponding author.
*E-mail address:* huangming05@fzu.edu.cn (M. Huang).
Peer review under responsibility of Institute of Rock and Soil Mechanics, Chinese Academy of Sciences.

https://doi.org/10.1016/j.jrmge.2024.12.018

(Yang et al., 2016; Zhang et al., 2017; Xu et al., 2024). Recent advancements in artificial intelligence (AI) methods offer significant potential to address these complex, nonlinear problems. AI models have demonstrated success in predicting and classifying geological conditions into various meaningful categories (Liu et al., 2020; Guo et al., 2023). By understanding the surrounding soil mass, engineers can make informed decisions to manage shield tunneling operations effectively.

Researchers have employed various machine learning (ML) methods such as support vector regression (Liu et al., 2019), support vector classifiers (Zhang et al., 2019), AdaBoost (Liu et al., 2020), deep neural networks (Wu et al., 2021), and long short-term memory networks (Liu et al., 2021), to explore the underlying relationships between shield machine monitoring data and geological conditions (Guo et al., 2023; Lai et al., 2023; Jiang et al., 2024). Recently, Yan et al. (2022) presented a framework for predicting geological conditions in shield tunneling by integrating a stacking classification algorithm with grid search and K-fold cross-validation. Xu et al. (2023) compared the performance of various algorithms, including multi-objective random forest, single-objective-AdaBoost, and suppressor chain-AdaBoost, for predicting geological conditions in super-large diameter slurry pressure balanced shield tunnels. These supervised ML models exhibit strong capabilities in nonlinear mapping, leveraging vast amounts of monitoring data to predict geological conditions accurately. However, they face several limitations: (1) supervised ML models require actual geological conditions as labeled inputs, which are often difficult and resource-intensive to obtain in practice; (2) conventional ML models lack the capability for continuous learning, making them challenging to adapt to new input data. On the one hand, manually assigning labels to raw data to develop a learning base is typically time-consuming. Additionally, it can be difficult to obtain accurate geological conditions for shield tunnel projects in complex construction. Therefore, an ML model that does not rely on labeled data to effectively predict the geological conditions of shield tunnels is necessary. On the other hand, the trained model typically only performs well for a specific boundary problem. When applying ML model to the new, unseen data, it needs to be retrained (Qian et al., 2021b). This is particularly the case for predicting geological conditions in shield tunneling. Consequently, developing techniques that can minimize the cost associated with retraining ML models is essential, enabling them to effectively adapt to new data.

Clustering algorithms present a promising alternative for predicting geological conditions during shield tunneling by classifying unlabeled data into interpretable structures (Zhou et al., 2019b; Wu et al., 2021; Pan et al., 2023). These algorithms may be more suitable for real-time applications where geological conditions are not readily available (Ikotun et al., 2023; Pan et al., 2023). The nonlinear relationship between shield tunneling machine monitoring data and geological conditions using clustering algorithms has been explored in several studies (Zhou et al., 2019b; Pan and Zhang, 2022; Yin et al., 2022). While significant progress has been made, these efforts mainly focus on identifying natural groupings within the data, with limited attention to temporal patterns in shield machine monitoring data. Time series clustering algorithms hold considerable potential for predicting geological conditions in shield tunneling operations. The deep temporal clustering (DTC) model is particularly well-suited for analyzing multivariate and complex time series data, such as that generated by shield machine monitoring. This model effectively reduces data dimensionality and learns temporal correlations between time series through the integration of one-dimensional convolutional neural network (1D CNN) and bidirectional long short-term memory (Bi-LSTM) layers, enabling precise clustering of multivariate time series data.

Integrating incremental learning can significantly enhance a clustering model's ability to learn from new data (Zhao et al., 2023). The approach allows the model to update its parameters based on new data inputs without requiring complete retraining, thereby mitigating the risk of performance degradation and avoiding time-consuming retraining processes. The elastic weight consolidation (EWC) method can be flexibly applied to various types of ML models and tasks without significant changes to the model structure. Additionally, EWC is designed to address the issue of catastrophic forgetting, a phenomenon where previously acquired knowledge is lost after training on new data. Preventing catastrophic forgetting during the incremental learning process helps maintain the model's performance stability during continuous learning.

This study proposes a novel approach by developing a DTC model combined with the EWC incremental learning method. First, the model employs the Boruta algorithm to select the most relevant features for training. Second, the DTC model is trained on a shield tunneling dataset from a metro project in Nanjing, China, and its performance is compared with nine time-series clustering algorithms (e.g., DTW-Kmeans, DTW-Kmedoids, and K-shape). Third, the continuous learning capability of the model is enhanced by integrating it with the EWC incremental learning method. Fourth, detailed feature importance is conducted, using the feature elimination method and the Shapley additive explanations (SHAP) method to determine the relative significance of each feature in predicting geological conditions. Finally, the DTC model is applied to the Xiamen metro shield tunnel dataset. In summary, the model can accurately predict geological conditions in real-time during shield tunneling without relying on actual geological data as input and demonstrates robust continuous learning capabilities.

## 2. Methodology

In this study, the DTC model is employed to predict geological conditions during shield tunneling. To enhance the model's continuous learning capability and enable real-time prediction of geological conditions, the parameters of the DTC model are updated using the EWC method. Fig. 1 presents the flowchart detailing the model development process. This section provides an overview of the Boruta feature selection algorithm, the DTC model, and the EWC method.

### 2.1. Boruta algorithm

The Boruta algorithm is an extension of the random forest algorithm (Kursa and Rudnicki, 2010). It enhances feature selection by introducing additional randomness. The key steps of the algorithm are: (1) Shuffling original features to create shadow features and concatenating them with the original features to form the training feature matrix; (2) Calculating the importance of each

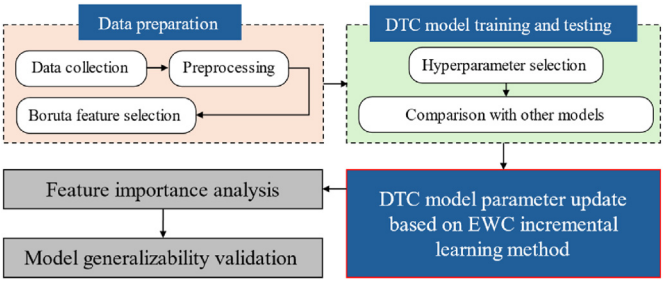


**Fig. 1.** Flowchart illustrates the implementation procedure of the developed model.

feature within the predictive model; (3) Computing Z-scores ($Z_{score}$) for both original and shadow features and determining the maximum Z-score ($Z_{max}$) among the shadow features; (4) Identify "important features" as those with a $Z_{score}$ greater than $Z_{max}$ and label features with a $Z_{score}$ less than $Z_{max}$ as "unimportant," subsequently removing them; and (5) Repeating the process until all features are classified as either "important" or "unimportant."

### 2.2. Deep temporal clustering (DTC)

The DTC model is a combination of deep learning and clustering algorithms designed to enhance the capability of handling time-series data (Sai Madiraju et al., 2018). The objective of the DTC model is to integrate dimensionality reduction and time-series clustering into a completely unsupervised end-to-end learning framework. This framework includes an encoder, a decoder, and a time-series clustering layer, as shown in Fig. 2.

#### 2.2.1. Model training process

Consider $n$ unlabeled instances, $x_1$, …, $x_n$, of a temporal sequence $x$. The goal is to perform unsupervised clustering of these $n$ unlabeled sequences into $k \leq n$ clusters, based on the latent high-level features of $x$. The input sequences are passed through a one-dimensional convolutional layer to capture short-range fluctuations within the sequences. Subsequently, a max pooling layer with a pool size of $P$ is applied for dimensionality reduction. This procedure compresses the input time-series data into a compact vector representation while maintaining the structural information inherent in the sequences.

Next, the output of the max pooling layer is input into a Bidirectional LSTM (Bi-LSTM). The LSTM network captures sequence patterns in both directions, compressing the input sequence into a more compact latent representation. The encoder structure is illustrated by the blue box in Fig. 2. The latent representation is then subjected to UpSample and deconvolution operations, reconstructing a time-series input while undergoing self-training to ensure the effectiveness of the autoencoder layer, as shown in the red box of Fig. 2.

Finally, the clustering layer assigns the Bi-LSTM latent representation of sequences $x_i$, $i = 1 \ldots n$, to clusters. Learning in the 1D CNN and Bi-LSTM involves minimizing two interleaved cost functions. The first is the mean square error (MSE) of the input sequence reconstruction from the Bi-LSTM's latent representation. The second is a clustering metric (e.g. KL divergence), which adjusts the weights in both the Bi-LSTM and CNN. This process enables the Bi-LSTM to encode high-level features that optimally separate the sequences into clusters, clarifying the spatiotemporal dynamics of $x$.

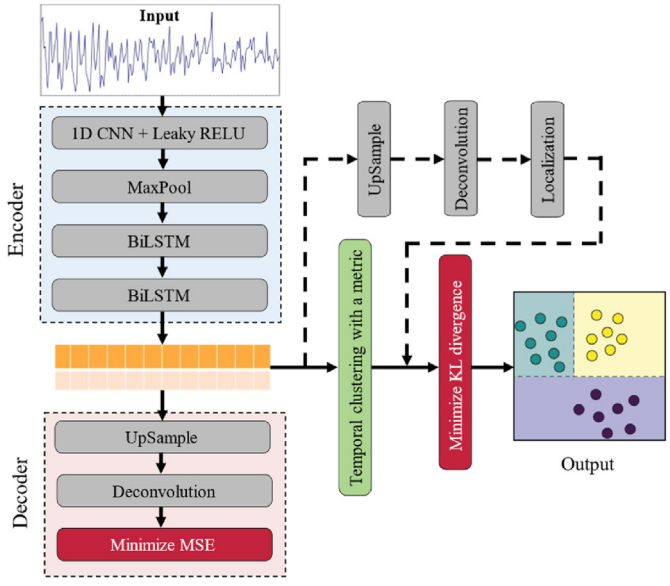


**Fig. 2.** Structure of the DTC model.

#### 2.2.2. Temporal clustering layer

The temporal clustering layer consists of $k$ centroids $\omega_j, j \in 1 \ldots k$. The input $x$ is transformed into latent signals $z_i$ through the encoder-decoder layer. $z_i$ is then used to perform hierarchical clustering with complete linkage in the feature space $Z$ through a similarity metric. We perform $k$ cut to obtain the clusters and then average the elements in each cluster to get initial centroids estimates $\omega_j, j \in 1 \ldots k$.

After initializing the centroids, the first step is to calculate the assignment probability of the input $x_i$ to cluster $j$. The assignment probability of the input's latent representation $z_i$ to cluster $j$ is higher when $z_i$ is closer to the centroid $\omega_j$ of that cluster. The calculation formula for the assignment probability is as follows:

$$q_{ij} = \frac{(1+\delta)^{-\frac{\psi+1}{2}}}{\sum_{j=1}^{k}(1+\delta)^{-\frac{\psi+1}{2}}} = \frac{\left(1+\frac{simil(z_i,\omega_j)}{\omega}\right)^{-\psi+1/2}}{\sum_{j=1}^{k}\left(1+\frac{simil(z_i,\omega_j)}{\omega}\right)^{-\psi+1/2}} \quad (1)$$

where $z_i$ is the signal in the latent space $Z$, obtained from the temporal autoencoder after encoding the input signal $x_i \in X$, $\psi$ is the number of degrees of freedom of the student's $t$ distribution, and $simil(z_i, \omega_j)$ is the similarity metric.

The DTC model provides four similarity measurement methods: complexity invariant similarity (CID), correlation-based similarity (COR), autocorrelation-based similarity (ACF), and Euclidean (EUCL). To train the temporal clustering layer, the optimization objective is set to minimize the KL divergence loss between the assignment probability $q_{ij}$ and the target distribution $p_{ij}$. $p$ is used to strengthen high-confidence predictions and normalize the losses to prevent distortion of the latent representation, as shown in Eq. (2). The formula for KL divergence loss is

$$p_{ij} = \frac{\lambda_j}{\sum_{j=1}^{k}\lambda_j} \quad (2)$$

$$L = \sum_{i=1}^{n}\sum_{j=1}^{k} p_{ij}\log\frac{p_{ij}}{q_{ij}} \quad (3)$$

where $f_j = \sum_{i=1}^{n} q_{ij}$, $\lambda_j = q_{ij}^2 / f_j$, $n$ and $k$ are the number of samples in the dataset and the number of clusters respectively.

The optimization in the DTC model involves batch-wise joint optimization of clustering and autoencoder tasks. First, the parameters of the autoencoder are pre-trained. After the pre-training phase, the clustering centers are initialized using hierarchical clustering. Subsequently, the autoencoder weights and cluster centers are updated using the gradients $dL_c/dz_i$ and $dL_{ae}/dz$, respectively:

$$\frac{dL_c}{d\omega_i} = \frac{\partial}{1+\partial}\sum_j\left(1+\frac{simil(z_i,\omega_j)}{\partial}\right)*\left(p_{ij}-q_{ij}\right)\frac{d(simil(z_i,\omega_j))}{d\omega_i} \quad (4)$$

$$\frac{dL_{ae}}{dz} = \frac{d\left(\frac{1}{2}\|x - x'\|_2^2\right)}{dz} \tag{5}$$

where $dL_c$ is the loss of classification and $dL_{ae}$ is the loss of autoencoder.

### 2.3. Elastic weight consolidation (EWC)

EWC enables the model to retain its knowledge of old tasks while learning new tasks, thus preventing catastrophic forgetting from occurring (Kirkpatricka et al., 2017). During the learning of a new task B, EWC constrains the important parameter $\theta$ to remain within a low-error region centered around the data distribution $\theta_A^*$ of the old task A, thereby preserving the performance of task A. The conditional probability can be calculated based on the prior probability $p(\theta)$ of the parameters and the probability $p(\theta|D)$ of the data as follows:

$$\log p(\theta|D) = \log p(\theta|D) + \log p(\theta) - \log p(D) \tag{6}$$

Assuming that the data is divided into two independent parts, one defined as Task A ($D_A$) and the other as task B ($D_B$), the equation can be rewritten as follows:

$$\log p(\theta|D) = \log p(\theta_B|D) + \log p(\theta|D_A) - \log p(D_B) \tag{7}$$

The posterior probability can be approximated as a Gaussian distribution. The function $L$ that we minimize in EWC is

$$L(\theta) = L_B(\theta) + \sum_i \frac{\lambda}{2} F_i \left(\theta_i - \theta_{A,i}^*\right)^2 \tag{8}$$

where $L_B(\theta)$ is the loss for task B only, $\lambda$ sets how important the old task is compared with the new one, $i$ labels each parameter, and $F$ is the Fisher information matrix.

## 3. Model development

### 3.1. Project description

This study utilizes data from an EPB shield tunneling project in Nanjing, Southeast China, to develop the ML model. The shield tunnel features both double-bore and single-lane designs. The construction area spans a total length of 1.9 km from DK65 + 866.421 to DK67 + 759.653, with a maximum buried depth of 21.38 m. The diameter of the shield cutterhead is 6500 mm, operating with an opening rate of 32%. The cutterhead rotation speed ranged from 0 to 3.05 rpm, with a torque of 5631 kN m. The maximum thrust force applied is 41,600 kN, and the maximum advance speed is set at 80 mm/min.

During the construction of tunnel segments 297–309, incorrect geological conditions assessments resulted in spoil buildup due to inadequate adjustments in conveyor speed and water flow, causing significant progress delays. The geological conditions were initially reported as moderately weathered muddy sandstone, but the actual soil was primarily silty clay. This discrepancy is expected, given that the spatial limitations of borehole drilling often hinder a comprehensive assessment of the actual geological conditions. Since supervised learning relies heavily on the quality and accuracy of labeled data, it may result in poor performance and unreliable predictions. Therefore, this study aims to use an unsupervised clustering algorithm to predict geological conditions. The proposed algorithm can group similar data sequences into clusters without requiring actual geological conditions as labeled input.

To reduce the impact of inaccurate geological conditions on the unsupervised clustering model's evaluation, excavation segments where the actual geological conditions differed from those reported in the geotechnical investigation were excluded. Instead, excavation segments with accurately reported geotechnical conditions were selected for the study dataset. The shield tunnel data includes silty clay (SC), plasticized silty clay (PSC), moderately weathered muddy sandstone (MWMS), and strongly weathered muddy sandstone (SWMS), as shown in Table 1.

### 3.2. Data collection and feature selection

Various parameters are monitored and recorded by sensors during the shield tunneling construction process. In this study, over 60,000 samples were collected as the dataset. Given the substantial variability in recorded data across different dimensions, the data was normalized using the minimum-maximum scaling method.

The selection of input features is critical for improving the predictive accuracy and reducing the computational complexity of the model. Firstly, based on previous studies (Liu et al., 2019, 2020; Chen et al., 2021), seventeen parameters with high relevance to predict geological conditions were selected. These include the total thrust (TT), cutterhead torque (CT), cutterhead rotational speed (CRS), earth chamber pressure (CP), advance speed (AS), thrust jack pressure (TJP), screw conveyer pressure (SCP), screw conveyer rotational speed (SCRS), horizontal deviation of the shield machine head (HDSH), horizontal deviation of the shield machine tail (HDST), vertical deviation of the shield machine head (VDSH), vertical deviation of the shield machine tail (VDST), rotation angle of the shield machine (RA), average water flow (AWF), grouting volume (GV), the helix angle of the shield machine (HA), and average bubble flow (ABF).

Next, the Boruta algorithm was used to refine the selection of input features. The results are illustrated in Fig. 3. The RA, AWF, GV, HA, and ABF were found to have a minimal impact on the predictive results, with $Z_{score}$ values lower than the shadow feature (*ShaMax*). Like most feature selection algorithms, the Boruta algorithm evaluates feature importance based primarily on the correlation between data. GV, AWF, and ABF exhibit more outliers and missing values, often due to sensor failures, which can obscure the true relationship between features and target variables. Although the Boruta algorithm is effective for feature selection, it may not capture all significant nonlinear relationships and can be sensitive to noise in the data. The final model input is $X = [CP, VDST, CRS, HDST, VDSH, TT, HDST, AS, TJP, SCRS, SCP, CT]^T$. A statistical overview of the model input features is depicted in Fig. 4.

### 3.3. Hyperparameter selection and evaluation metrics

The dataset was divided into two distinct parts: 70% of the data is used for training, validation, and testing of the DTC model, while the remaining 30% is reserved for evaluating the EWC incremental learning method. The hyperparameters search space for the DTC model is clearly defined, and the optimal set of hyperparameters was determined using a grid search approach, as detailed in Table 2. Additionally, the influence of the input sequence length and the number of clusters on the model's performance will be analyzed in detail in the subsequent section. The experiments were conducted on a platform equipped with an NVIDIA Tesla P100 GPU and 64 GB DDR4 RAM, utilizing a PyTorch 1.8 and Python 3.8 environment.

The evaluation metrics used in this study are the adjusted Rand index (ARI), normalized mutual information (NMI), and accuracy rate (ACC) (Aghabozorgi et al., 2015; Pan et al., 2023). These metrics compare the clustering results with the actual geological conditions to assess the quality of the discovered clusters. The ARI is employed

**Table 1**
Geological conditions in the study area.

| Ring number | 12–238 | 259–287 | 345–623 | 652–771 | 853–956 |
|---|---|---|---|---|---|
| Length (m) | 226 | 28 | 278 | 119 | 103 |
| Stratum | Silty clay (SC) | Plasticized silty clay (PSC) | Moderately weathered muddy sandstone (MWMS) | Strongly weathered muddy sandstone (SWMS) | MWMS |

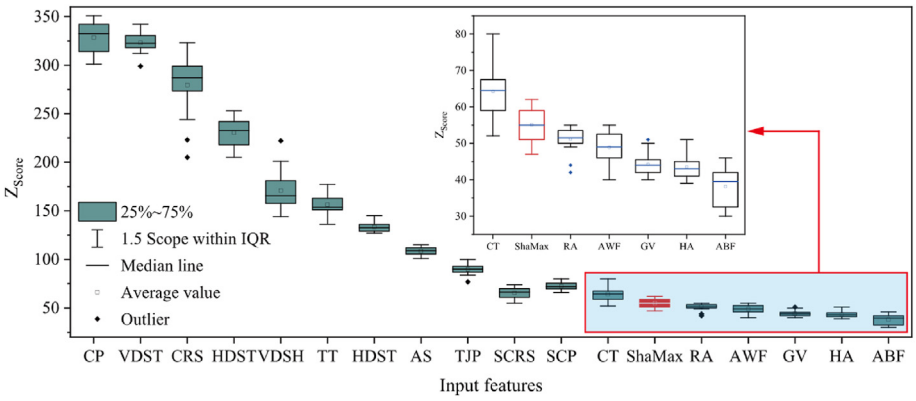


**Fig. 3.** Results of the Boruta algorithm.

to assess the similarity between two clusters, with values ranging from −1 to 1:

$$ARI = \frac{RI - \overline{RI}}{RI_{Max} - \overline{RI}} \tag{9}$$

where $RI$ represents the Rand index, calculated as $\overline{RI}$. $\overline{RI}$ is the expected value of the Rand index under random clustering conditions, and $RI_{Max}$ denotes the maximum value of the Rand index:

$$RI = \frac{TP + TN}{TP + FP + FN + TN} \tag{10}$$

where a true positive (TP) is an instance where the algorithm's prediction aligns with the actual positive cluster. A true negative (TN) is an instance where the prediction and the actual cluster are both negative. A false positive (FP) arises when the algorithm incorrectly predicts an actual negative instance to a positive cluster. A false negative (FN) arises when the algorithm incorrectly predicts a positive instance to a negative cluster.

The NMI is an evaluation metric based on information theory, that measures the level of information shared between the clustering results and the true labels. Its values range from 0 to 1:

$$NMI(U,V) = \frac{2MI(U,V)}{H(U) + H(V)} \tag{11}$$

where $U$ represents the true clustering labels, and $V$ is the clustering labels generated by the algorithm; $MI(U,V)$ is the mutual information between $U$ and $V$; $H(U)$ represents the entropy of $U$, and $H(V)$ represents the entropy of $V$. The ACC is defined as the ratio of correctly predicted instances to the total number of instances, with values ranging from 0 to 1.

The dataset in this study contains four types of geological conditions, as shown in Table 1. If the model can classify the dataset into four clusters corresponding to these geological conditions, the model can be considered to be effective in identifying geological conditions. Each input sequence is associated with a corresponding ring number (Table 1), which determines the true geological condition of that input sequence. A comparison of the model's predicted results with the actual geological conditions will verify whether the input sequences have been correctly clustered.

## 4. Results and discussion

### 4.1. Performance of the clustering models

#### 4.1.1. Influence of input sequence length

Preliminary experiments were conducted to determine the optimal sequence length that maximizes predictive accuracy. These experiments indicated that the model performs best with input sequence lengths in the range of 24–104. Therefore, input sequence lengths of 24, 44, 64, 84, and 104 were further evaluated, as shown in Fig. 5. It can be found that the model achieves optimal clustering performance at an input sequence length of 64, with the highest values of ACC, NMI, and ARI. Choosing an input sequence length of 64 is reasonable, as it does not exceed the typical number of data points recorded for one ring of segments. The dataset was recorded at a frequency of 60 s per trip, with an average of 67 data points collected per ring of a tunnel segment. Using model input sequences longer than 67 data points may result in sequences containing data points from two successive rings of tunnel segments. This is suboptimal, as the two successive rings are not continuous in time due to the intervening segment assembly stage.

#### 4.1.2. Influence of the number of clusters

The number of clusters refers to the groups identified or selected during a cluster analysis. According to Table 3, the DTC model demonstrates optimal performance for the case with four clusters, achieving a prediction accuracy of ACC = 75.1%. The accuracy declines to 69.9% with three clusters and further declines to 57.5% with five clusters. Similarly, other performance metrics, such as NMI and ARI, exhibit the same trend.

The clustering results for AS and TJP are shown in Figs. 6 and 7, respectively. The color of the line represents the true geological condition associated with each input sequence. For example, Fig. 6a and 7a show all input sequences classified by the model as SC. When all the lines are red, indicating that the model achieved 100% accuracy in predicting the SC stratum.

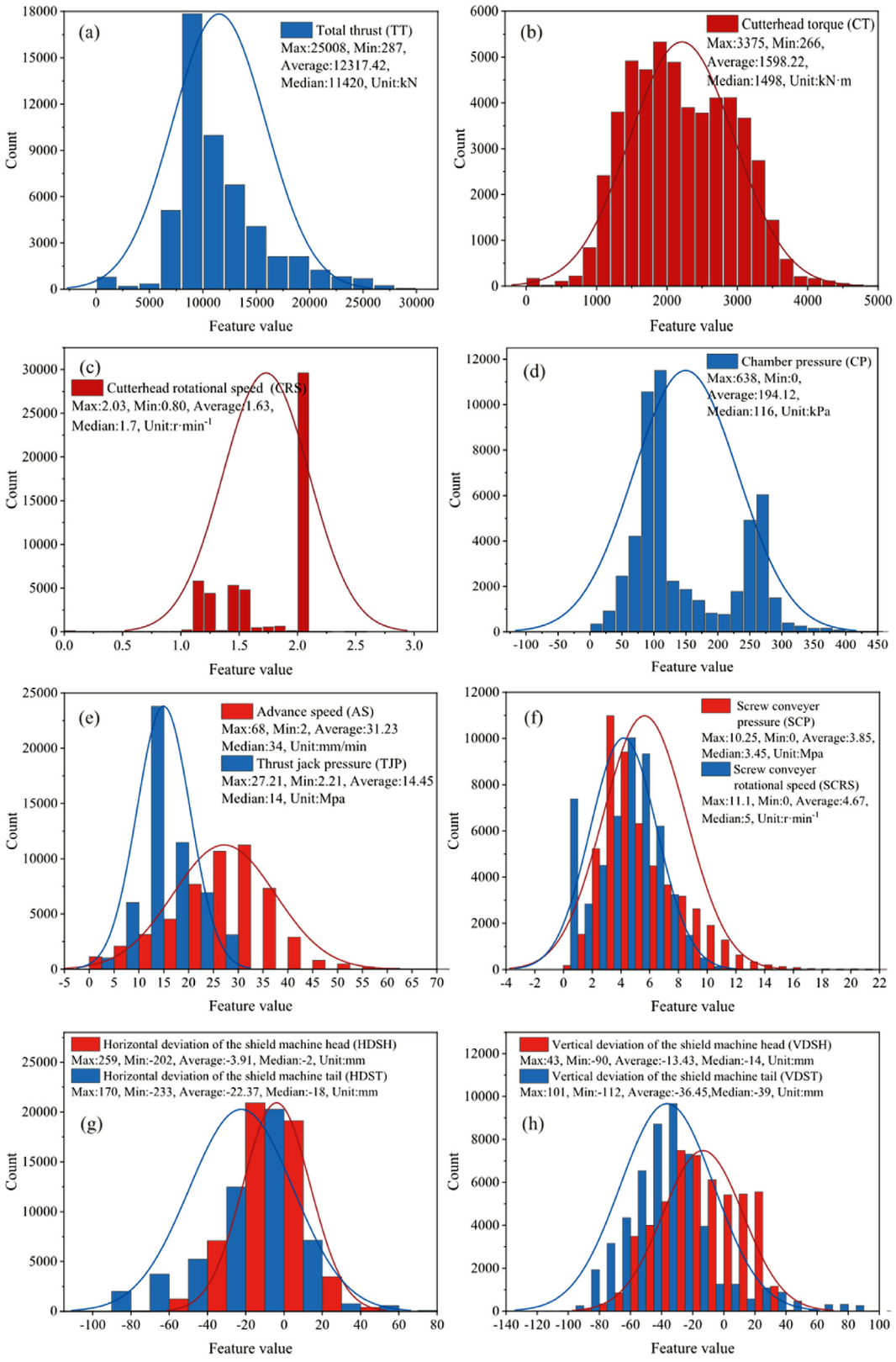


**Fig. 4.** Data distribution: (a) TT, (b) CT, (c) CRS, (d) CP, (e) AS and JTP, (f) SCP and SCRS, (g) HDSH and HDST, and (h) VDSH and VDST.

The main diagonal elements in Fig. 8 indicate the number of input sequences that were correctly clustered. For instance, 251 out of 261 input sequences from the SC stratum were accurately identified, resulting in an accuracy rate of 96.16%. Among the 465 input sequences from the MWMS stratum, 372 were correctly identified, resulting in an accuracy rate of 80%. However, all 18

**Table 2**
Hyperparameter search space and optimal settings for the DTC model.

| Hyperparameter | Search space | Optimal hyperparameter |
|---|---|---|
| Number of clusters | [2, 3, 4, 5, 6] | 4 |
| Number of layers[a] | [6, 8, 10] | 8 |
| Batch size | [64, 128, 256] | 256 |
| Learning rate | [0.01, 0.1] | 0.01 |
| Epoch | [25, 50, 100] | 50 |
| Input sequence lengths | [24, 44, 64, 84, 104] | 64 |

Note: a is the number of units in the BiLSTM layers.

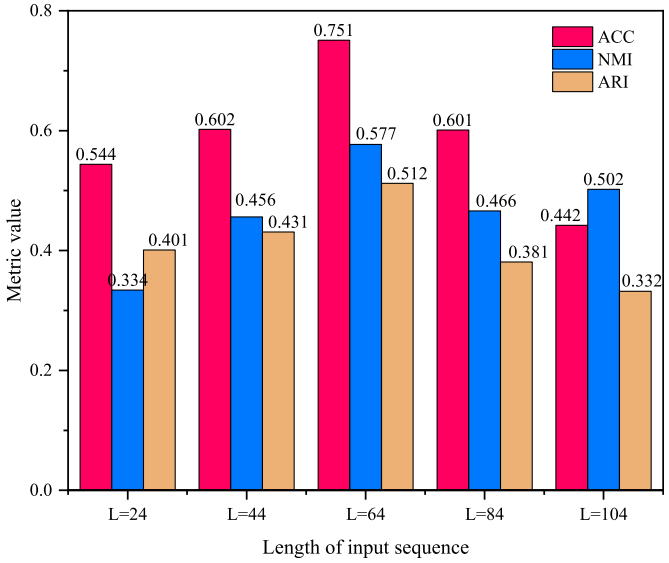


**Fig. 5.** Model performance with different input sequence lengths (number of clusters = 4).

**Table 3**
DTC model clustering results.

| Model | Evaluation | Number of clusters | | | | |
|---|---|---|---|---|---|---|
| | | 2 | 3 | 4 | 5 | 6 |
| DTC | ACC | 0.619 | 0.699 | **0.751** | 0.575 | 0.55 |
| | NMI | 0.182 | 0.495 | **0.577** | 0.352 | 0.018 |
| | ARI | 0.134 | 0.391 | **0.512** | 0.312 | 0.05 |

Note: The text in bold indicates optimal performance.

input sequences from the PSC stratum were incorrectly identified as SC. Additionally, out of the 103 inputs sequences from the SWMS stratum, 85 were misclassified as MWMS. These misidentifications can be attributed to the similarities in soil parameters between the PSC and SC strata, as well as between the MWMS and SWMS strata. This similarity leads to an almost identical distribution of shield control data across these strata. As shown in Fig. 9, the distribution of the four shield tunneling control parameters, namely CT, TT, SCP, and JTP reveals significant overlap and considerable similarity.

#### 4.1.3. Comparison with the nine clustering models

To validate the effectiveness of the DTC model, nine widely used time series clustering algorithms were selected for comparison. The performance of these comparison models was evaluated with different numbers of clusters, as shown in Table 4. The results indicate that the DTC model is optimal with four clusters, achieving an ACC of 0.751, NMI of 0.577, and ARI of 0.512.

The DTW-Kspectral, SoftDTW-Kmeans, and SoftDTW-Kspectral models perform optimally with only two clusters. This suggests that these models tend to divide the dataset into two clusters and are unable to effectively distinguish the four geological conditions. The DTC model demonstrates superior performance compared to the other models for both three and four clusters, showing that the DTC model is more capable of identifying similar strata and can effectively identify the third and fourth strata within the dataset. This is because the DTC model can explore potential correlations within the input data through its integrated LSTM layer, thereby enabling it to more accurately identify subtle differences between various input sequences. This capability significantly enhances the DTC model's performance compared to those of conventional clustering methods, such as DTW-Kmeans and DTW-Kmedoids. However, high similarity among geological conditions can lead to inaccurate identification by the DTC model. In addition, compared to supervised machine learning models, clustering models, which lack explicit goals or labeled data to guide learning, may exhibit reduced reduction in prediction accuracy.

### 4.2. Performance of incremental learning

The DTC model was initially trained on 70% of the dataset referred to as the “old task”, as described in the previous section. In this section, the results of training the DTC model on the remaining 30% of the data using an incremental learning method, referred to as the “new task” is presented. The new task was divided into 39 inputs, signifying that the DTC model's parameters were updated 39 times through the EWC method. A significant challenge in incremental learning is the phenomenon known as “catastrophic forgetting,” where the introduction of new task data can significantly degrade the model's performance on previously learned tasks. To mitigate this issue, the performance of the updated DTC model on the old tasks is evaluated after undergoing incremental learning updates.

Three incremental learning strategies are applied to the DTC model: global fine-tuning, local fine-tuning, and EWC. The global fine-tuning method allows the model to update all its parameters for the new task, while the local fine-tuning method locks all parameters except those in the updated clustering layer. Fig. 10a–c demonstrated the improved performance of the DTC model with increasing input sequences, indicating its capability for continual updates with new data. Furthermore, Fig. 10d is a violin plot that illustrates the performance of the DTC model following 39 updates, demonstrating that the EWC method achieves the highest prediction accuracy.

The DTC model, after being updated using the three incremental learning strategies, was retrained on the old task to check for signs of catastrophic forgetting. Fig. 11a–c presents the improved performance of the DTC model on the old task. Fig. 11b shows that the local fine-tuning method results in a gradual decline in performance on the old task as the number of model updates increases, indicating the occurrence of catastrophic forgetting. Both the global fine-tuning (Fig. 11a) and the EWC (Fig. 11c) methods show fluctuations in model performance as the number of updates increases. However, the global fine-tuning method exhibits a significant decline in performance on old tasks, with accuracy fluctuating between 36.8% and 59.4%. In contrast, the EWC method maintains more stable performance across updates, with accuracy ranging from 68.9% to 80.5%. Notably, the accuracy of the DTC model updated with the EWC method performs best. Therefore, it can be concluded that the EWC method effectively mitigates catastrophic forgetting.

The lack of model parameter updates can lead to a significant decline in model performance when the model encounters previously unseen data, such as novel geological conditions encountered

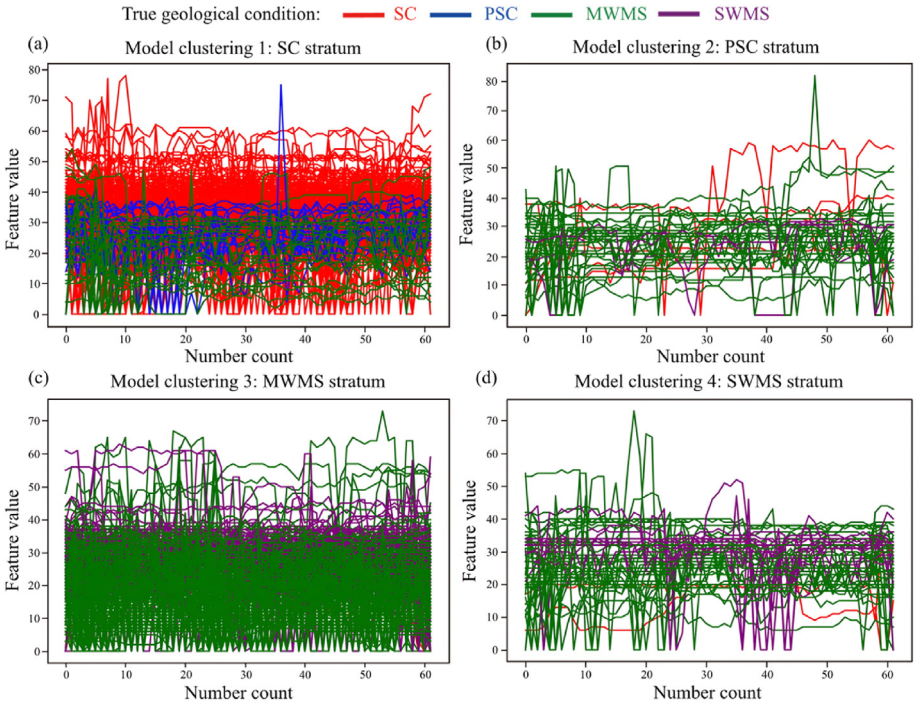


**Fig. 6.** DTC model clustering results for AS: model recognized as (a) SC stratum, (b) PSC stratum, (c) MWMS stratum, and (d) SWMS stratum.

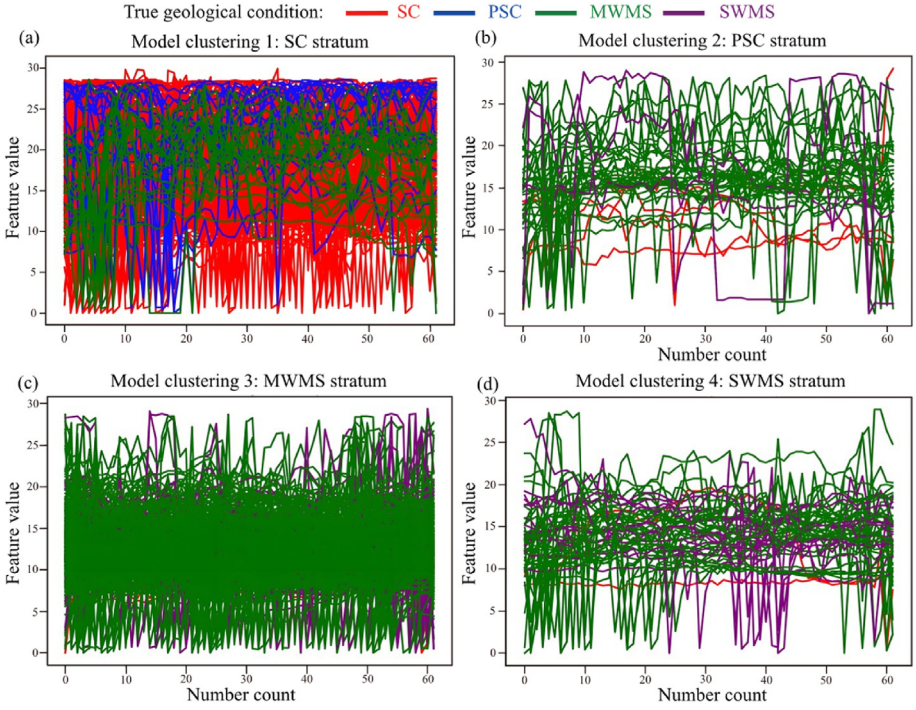


**Fig. 7.** DTC model clustering results for TJP: model recognized as (a) SC stratum, (b) PSC stratum, (c) MWMS stratum, and (d) SWMS stratum.

in practice. However, when training a model on new data, the old data typically needs to be integrated with the new data into a combined dataset and the model needs to be retrained. This process usually requires extended training time. In contrast, incremental learning methods allow an already trained model to be updated solely with new data, eliminating the need for complete retraining. This approach significantly reduces the time required for model training and is better suited to real-time geological condition prediction during shield tunneling.

The EWC method determines the relative importance of each feature in relation to the task being learned during the training process. By incorporating a regularization term into the loss function, EWC penalizes excessive changes to these crucial features, effectively preventing significant changes in model parameters

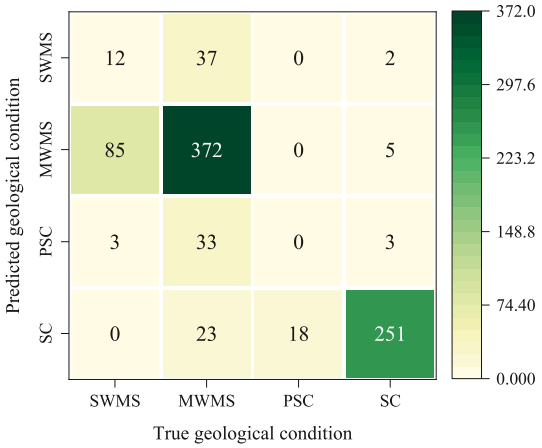


**Fig. 8.** Confusion matrix about the DTC model clustering results.

when new data is introduced. This reduces the risk of the model forgetting previously learned information. However, as the model expands, the computational burden associated with calculating the Fisher information matrix and applying constraint terms increases considerably.

### 4.3. Importance analysis of input features

Understanding how the 12 input features influence prediction outcomes is inherently challenging due to the semi-transparent nature of ML models. To assess the effect of each input feature on the model's performance, a feature elimination method was applied, where one feature was excluded in each combination. The results of this process are presented in Fig. 12. The results show a decline in performance when key features such as CP, CRS, VDST, HDST, VDSH, and HDSH are excluded. However, removing features like TT, CT, SCP, TJP, and SCRS has minimal effect on performance.

The SHAP method is also used to evaluate the importance of features. It is worth noting that the SHAP method cannot be directly applied to time-series clustering models. Accordingly, we constructed an LSTM model as a predictor for the SHAP method. The LSTM model, a supervised machine learning algorithm, achieved a prediction accuracy of approximately 88.2%. This approach enables an investigation of the influence of different input features on the model's prediction of geological conditions from both supervised and unsupervised ML perspectives. Fig. 13 shows that CRS has the largest influence on the prediction results, and it is followed by other significant features such as CP, VDST, HDST, VDSH, and HDSH. The findings support the outcome of the previous analysis of the feature elimination method.

The influence of individual input features on the model's output is presented in Fig. 14, where SHAP values are plotted on the x-axis and the input features on the y-axis. A higher SHAP value indicates a stronger positive impact on the prediction outcomes. The color coding of the points reflects the magnitude of the original values for each sample. The graph reveals that smaller CRS values promote the model's prediction results for SC and PSC strata. Conversely, larger CRS values improve the prediction results for MWMS and SWMS strata, which are rock strata requiring a higher cutterhead rotational speed for effective cutting compared to the clay formations. Larger CP values promote the model's prediction results for SC and PSC strata, while smaller CP values promote the prediction results for MWMS and SWMS strata. This is because clay strata have poorer face stability, requiring higher CP values for stability.

## 5. Generalization

The validity and generalization of the DTC model were further verified using the EPB shield tunneling monitoring dataset from the Xiamen metro line 3 project in China. The geology of the Xiamen project consists mainly of residual gravelly clayey soil, silty clay and medium weathered granite. Data processing ensures that the types and numbers of input features in the DTC model for the Xiamen

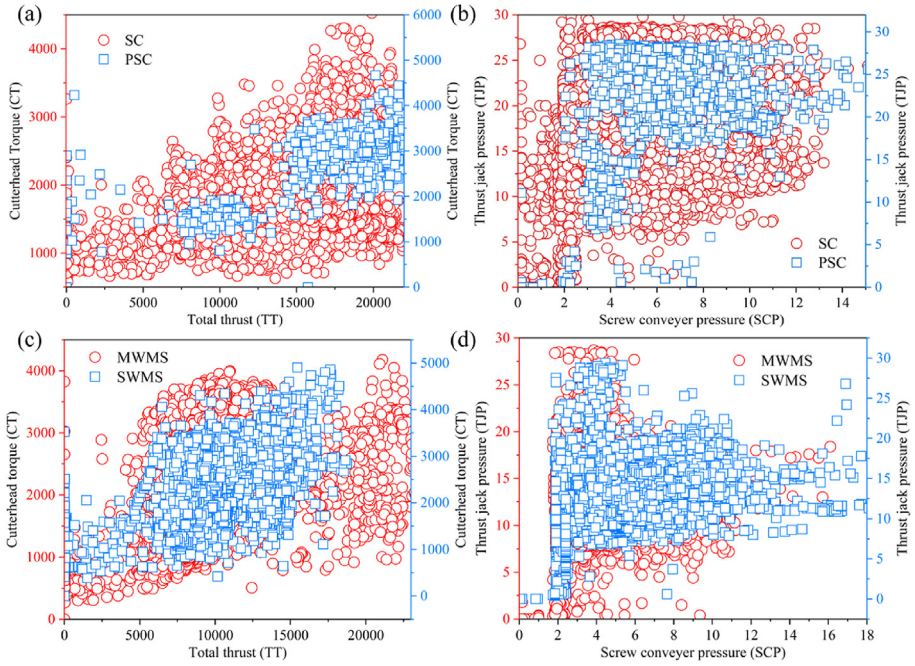


**Fig. 9.** Scatter plot of model input features: (a) TT and CT in the SC and PSC stratum, (b) SCP and TJP in the SC and PSC stratum, (c) TT and CT in the MWMS and SWMS stratum, and (d) SCP and JTP in the MWMS and SWMS stratum.

**Table 4**
Evaluation of clustering performance among different time series clustering algorithms.

| Model | Metric | Number of clusters | | | | | Model | Metric | Number of clusters | | | | |
|---|---|---|---|---|---|---|---|---|---|---|---|---|---|
| | | 2 | 3 | 4 | 5 | 6 | | | 2 | 3 | 4 | 5 | 6 |
| DTC | ACC | 0.619 | 0.699 | 0.751 | 0.575 | 0.55 | K-shape | ACC | 0.342 | 0.472 | 0.242 | 0.481 | 0.621 |
| | NMI | 0.382 | 0.455 | 0.577 | 0.352 | 0.018 | | NMI | 0.012 | 0.019 | 0.014 | 0.017 | 0.122 |
| | ARI | 0.234 | 0.391 | 0.512 | 0.312 | 0.05 | | ARI | 0.002 | 0.009 | 0.005 | 0.020 | 0.123 |
| DTW-Agglomerative | ACC | 0.6 | 0.612 | 0.603 | 0.535 | 0.421 | SoftDTW-Agglomerative | ACC | 0.614 | 0.619 | 0.591 | 0.553 | 0.542 |
| | NMI | 0.123 | 0.232 | 0.226 | 0.212 | 0.192 | | NMI | 0.132 | 0.243 | 0.252 | 0.255 | 0.259 |
| | ARI | 0.092 | 0.266 | 0.245 | 0.239 | 0.155 | | ARI | 0.102 | 0.252 | 0.242 | 0.212 | 0.208 |
| DTW-Kmeans | ACC | 0.632 | 0.642 | 0.613 | 0.543 | 0.512 | SoftDTW-Kmeans | ACC | 0.653 | 0.452 | 0.582 | 0.572 | 0.569 |
| | NMI | 0.157 | 0.264 | 0.262 | 0.261 | 0.263 | | NMI | 0.266 | 0.090 | 0.251 | 0.242 | 0.232 |
| | ARI | 0.154 | 0.291 | 0.280 | 0.216 | 0.211 | | ARI | 0.287 | 0.073 | 0.254 | 0.224 | 0.212 |
| DTW-Kmedoids | ACC | 0.532 | 0.633 | 0.452 | 0.451 | 0.352 | SoftDTW-Kmedoids | ACC | 0.523 | 0.543 | 0.525 | 0.492 | 0.509 |
| | NMI | 0.051 | 0.227 | 0.153 | 0.150 | 0.201 | | NMI | 0.002 | 0.026 | 0.018 | 0.009 | 0.008 |
| | ARI | 0.043 | 0.241 | 0.143 | 0.141 | 0.139 | | ARI | 0.003 | 0.012 | 0.009 | 0.008 | 0.013 |
| DTW-Kspectral | ACC | 0.450 | 0.352 | 0.282 | 0.241 | 0.221 | SoftDTW-Kspectral | ACC | 0.602 | 0.521 | 0.572 | 0.582 | 0.382 |
| | NMI | 0.003 | 0.001 | 0.002 | 0.002 | 0.003 | | NMI | 0.448 | 0.403 | 0.441 | 0.423 | 0.432 |
| | ARI | 0.011 | 0.004 | 0.003 | 0.021 | 0.022 | | ARI | 0.553 | 0.462 | 0.459 | 0.342 | 0.272 |

Note: The text in bold indicates optimal performance.

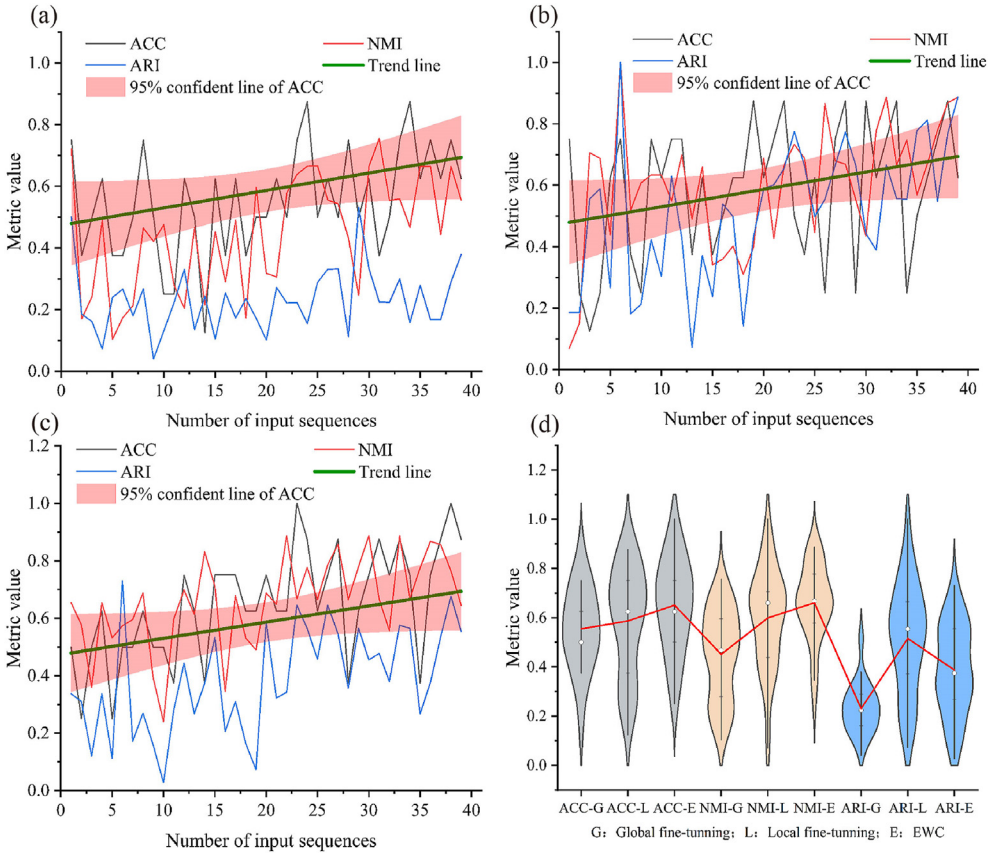


**Fig. 10.** Performance of DTC models based on incremental learning: (a) global fine-tuning method, (b) local fine-tuning method, (c) EWC method, and (d) violin charts for evaluation metrics.

dataset are consistent with those for the Nanjing dataset. Statistical information on the input features is shown in Table 5**.** Additionally, the model's hyperparameters are kept consistent with those in Table 2. While this may not provide globally optimal hyperparameters for the Xiamen dataset, it ensures a univariate comparison experiment.

The ACC of the DTC model on the Xiamen dataset is 81.13%, with NMI and ARI values of 0.6399 and 0.6242, respectively, further verifying the model's generalizability in different shield tunneling projects. Fig. 15 shows the confusion matrix of the DTC model's prediction results. The model achieves higher accuracy in predicting the RGCS and MWG strata, with 97.65% and 90.48%, respectively. However, the accuracy decreases to 60.27% and 75.31% for predicting the SC-FWG and SC strata, respectively.

The DTC model incorrectly predicted only two input sequences, SC-FWG and SC strata, when predicting RGCS. It incorrectly predicted five input sequences as SC-FWG strata and one sequence as SC strata when predicting MWG strata. This may be attributed to

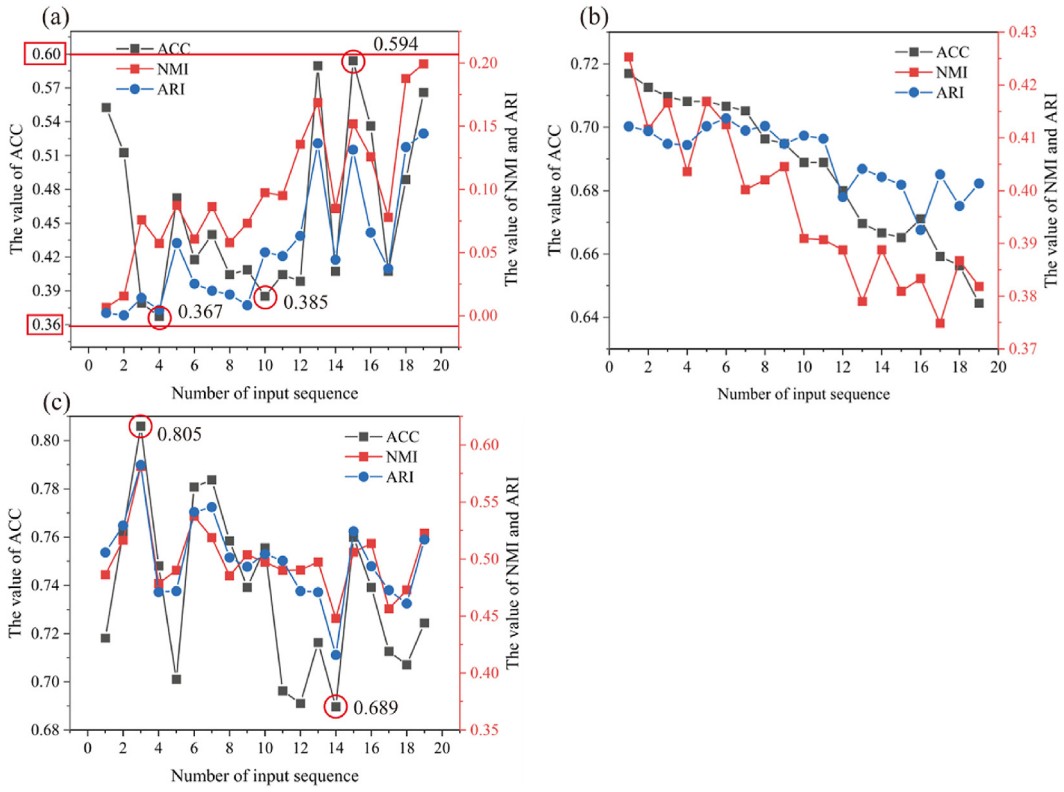


**Fig. 11.** Catastrophic forgetting evaluation of incremental learning methods: (a) global fine-tuning, (b) local fine-tuning, and (c) EWC.

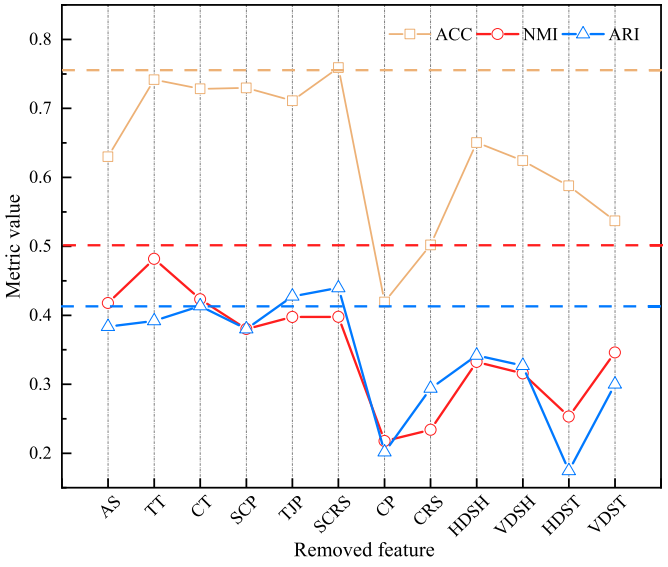


**Fig. 12.** Performance of the DTC model for different combinations of input parameters.

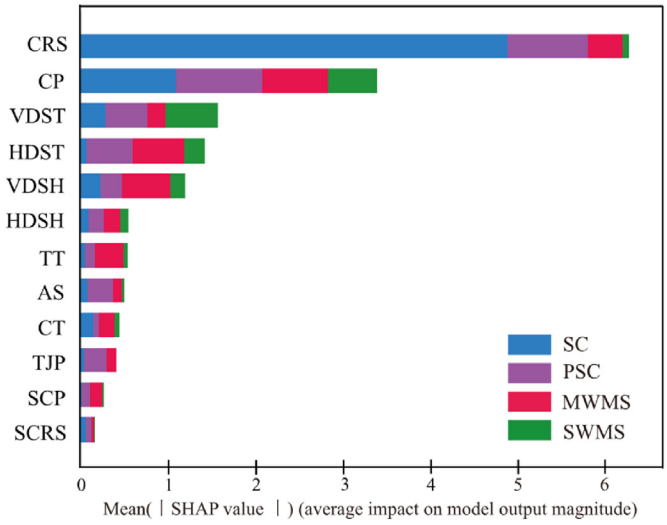


**Fig. 13.** Results of feature importance based on the SHAP method.

the uneven distribution of FWG in the tunnel face within the SC-FWG mixed strata, which closely resembles the MWG stratum. When predicting SC-FWG mixed strata, the model incorrectly classified 19 input sequences as SC strata and 10 as MWG strata. Additionally, the model incorrectly predicted 19 input sequences as SC-FWG mixed strata when predicting SC strata. These results highlight the limitations of the DTC model in distinguishing between similar and composite strata.

## 6. Conclusions

An unsupervised incremental learning model, combining deep temporal clustering (DTC) with elastic weight consolidation (EWC), has been developed in this study. The EWC-DTC model facilitated real-time prediction of geological conditions during EPB shield tunneling without needing labeled data. The main conclusions of this study are summarized as follows:

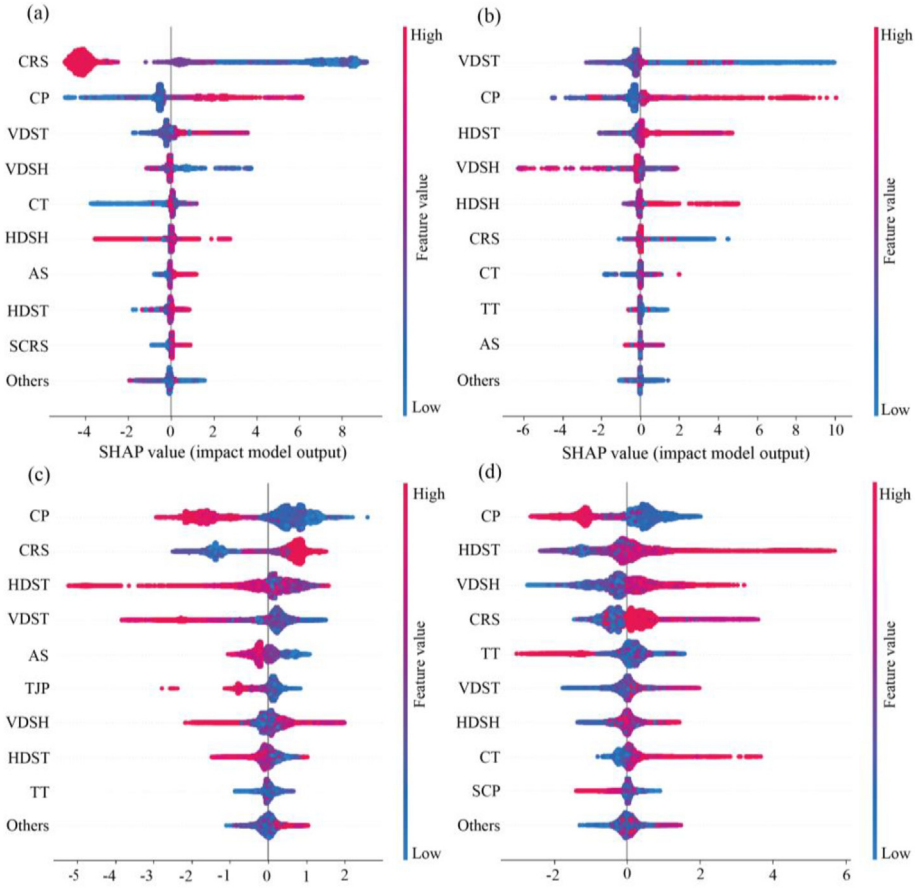


**Fig. 14.** Results of feature importance based on the SHAP method: (a) SC, (b) PSC, (c) MWMS, and (d) SWMS.

**Table 5**
Statistics of Xiamen project study area dataset.

| Parameter | Unit | Max | Min | Average | Median |
|---|---|---|---|---|---|
| Advance speed (AS) | mm/min | 38.12 | 6.72 | 25.33 | 27.98 |
| Total thrust (TT) | kN | 26259.71 | 6278.26 | 13424.16 | 12373.67 |
| Cutterhead torque (CT) | kN·m | 3736.34 | 953.40 | 2265.28 | 2422.89 |
| Screw conveyer pressure (SCP) | Mpa | 16.82 | 1.54 | 5.46 | 5.16 |
| Total jack pressure (TJP) | Mpa | 17.58 | 0 | 7.58 | 7.34 |
| Screw conveyer rotation speed (SCRS) | $r \cdot min^{-1}$ | 22.52 | 0 | 3.37 | 2.55 |
| Chamber pressure (CP) | kPa | 638.21 | 0 | 197.03 | 121.37 |
| Cutterhead rotation speed (CRS) | $r \cdot min^{-1}$ | 2.16 | 1.01 | 1.73 | 1.98 |
| Horizontal deviation of the shield head (HDSH) | mm | 219.72 | −206.51 | 3.64 | 4.34 |
| Vertical deviation of the shield head (VDSH) | mm | 87.81 | −212.74 | −18.83 | −23.13 |
| Horizontal deviation of the shield tail (HDST) | mm | 88.72 | −89.22 | −3.27 | −2.82 |
| Vertical deviation of the shield tail (VDST) | mm | 112.12 | −76.03 | −16.45 | −21.81 |

(1) The DTC model achieves a higher accuracy of 75.1% for the case study considered, outperforming the nine popular time series clustering models under the four clusters scenario. Additionally, the DTC model demonstrates excellent performance when applied to another project with an accuracy of 81.1%, highlighting the feasibility of employing an unsupervised clustering model for predicting the geological conditions during shield tunneling.

(2) The DTC model demonstrates an excellent ability to distinguish between widely differing geological conditions. However, a notable decrease in accuracy occurs when predicting similar geological conditions and composite strata. The DTC model demonstrates an accuracy of 96.16% in predicting the SC stratum, but most of the SWMS stratum was misclassified as MWMS. Additionally, the model achieves an accuracy of 97.65% for the RGCS stratum and 90.48% for the MWG stratum. The accuracy declines to 75.31% and 60.27% for predicting the SC and SC-FWG strata, respectively.

(3) The EWC method significantly enhances the continuous learning capability of the DTC model. By allowing the DTC model to learn from a continuous stream of data, EWC enables the DTC model to adaptively perceive geological conditions and update parameters ring by ring as tunneling progresses. Additionally, the ACC of the EWC-DTC model on old tasks ranges from 68.9% to 80.5%, indicating that the EWC-DTC model's ability to effectively mitigate catastrophic forgetting.

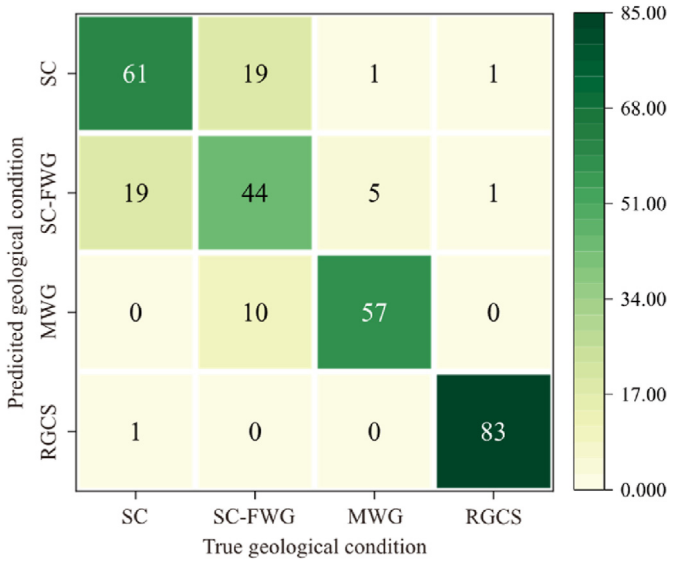


**Fig. 15.** Confusion matrix of the DTC model clustering results in the Xiamen dataset.

Despite potential reductions in prediction accuracy compared to supervised ML models due to the absence of labeled data, unsupervised learning offers a significant advantage in scenarios where accurate labels are unavailable. Future research can focus on two main areas: (1) improving the interpretability of ML models to better understand the complex interactions between shield tunneling parameters and geological conditions, and (2) enhancing clustering algorithms to improve model accuracy, especially in scenarios with high similarity among geological conditions.

## CRediT authorship contribution statement

**Jiajie Zhen:** Writing – review & editing, Writing – original draft, Visualization, Validation, Supervision, Software, Resources, Project administration, Methodology, Investigation, Funding acquisition, Formal analysis, Data curation, Conceptualization. **Fengwen Lai:** Writing – review & editing, Visualization, Validation, Supervision, Resources. **Jim S. Shiau:** Writing – review & editing. **Ming Huang:** Writing – review & editing, Visualization, Validation, Resources, Project administration. **Yao Lu:** Writing – review & editing. **Jinhua Lin:** Writing – review & editing, Resources, Project administration.

## Declaration of competing interest

The authors declare that they have no known competing financial interests or personal relationships that could have appeared to influence the work reported in this paper.

## Acknowledgments

This study is financially supported by the National Natural Science Foundation of China (Grant Nos. 52378392, 52408356) and Foal Eagle Program Youth Top-notch Talent Project of Fujian Province, China (Grant No. 00387088).

## References

Aghabozorgi, S., Shirkhorshidi, A.S., Teh Ying, W., 2015. Time-series clustering - a decade review. Inf. Syst. 53, 16–38.
Chen, H., Li, X., Feng, Z., Wang, L., Qin, Y., Skibniewski, M.J., Chen, Z.S., Liu, Y., 2023. Shield attitude prediction based on Bayesian-LGBM machine learning. Inf. Sci. 632, 105–129.
Chen, Z., Zhang, Y., Li, J., Li, X., Jing, L., 2021. Diagnosing tunnel collapse sections based on TBM tunneling big data and deep learning: a case study on the Yinsong Project, China. Tunn. Undergr. Space. Technol. 108, 103700.
Cheng, C., Ni, P.P., Zhao, W., Jia, P.J., Gao, S., Wang, Z.G., Deng, C.C., 2021. Face stability analysis of EPB shield tunnel in dense sand stratum considering the evolution of failure pattern. Comput. Geotech. 130, 103890.
Guo, S., Wang, B., Zhang, P., Wang, S., Guo, Z., Hou, X., 2023. Influence analysis and relationship evolution between construction parameters and ground settlements induced by shield tunneling under soil-rock mixed-face conditions. Tunn. Undergr. Space Technol. 134, 105020.
Huang, M., Lu, Y., Zhen, J., Lan, X., Xu, C., Yu, W., 2023. Analysis of face stability at the launch stage of shield or TBM tunnelling using a concrete box in complex urban environments. Tunn. Undergr. Space Technol. 135, 105067.
Ikotun, A.M., Ezugwu, A.E., Abualigah, L., Abuhaija, B., Heming, J., 2023. K-means clustering algorithms: a comprehensive review, variants analysis, and advances in the era of big data. Inf. Sci. 622, 178–210.
Jiang, Q.H., Zhang, J.Z., Zhang, D.M., Huang, H.W., Shi, J.K., Li, Z.L., 2024. Influence of geological uncertainty on longitudinal deformation of tunnel based on improved coupled Markov chain. Eng. Geol. 337, 107564.
Kirkpatricka, J., Pascanu, R., Rabinowitz, N., Veness, J., Desjardins, G., Rusu, A.A., Milan, K., Quan, J., Ramalho, T., Grabska-Barwinska, A., Hassabis, D., Clopath, C., Kumaran, D., Hadsell, R., 2017. Overcoming catastrophic forgetting in neural networks. Proc. Natl. Acad. Sci. U.S.A. 114 (13), 3521–3526.
Kursa, M.B., Rudnicki, W.R., 2010. Feature selection with the Boruta package. J. Stat. Software 36, 1–13.
Lai, F.W., Shiau, J., Keawsawasvong, S., Chen, F.Q., Banyong, R., Seehavong, S., 2023. Physics-based and data-driven modeling for stability evaluation of bried structures in natural clays. J. Rock Mech. Geotech. Eng. 15 (5), 1248–1262.
Lai, F.W., Tschuchnigg, F., Schweiger, H., Liu, S., Shiau, J., Cai, G., 2024. A numerical study of deep excavations adjacent to existing tunnels: integrating CPTU and SDMT to calibrate soil constitutive model. Can. Geotech. J. 1–52.
Li, S.C., Liu, B., Xu, X.J., Nie, L.C., Liu, Z.Y., Song, J., Sun, H.F., Chen, L., Fan, K.R., 2017. An overview of ahead geological prospecting in tunneling. Tunn. Undergr. Space. Technol. 63, 69–94.
Liu, B., Wang, R., Guan, Z., Li, J., Xu, Z., Guo, X., Wang, Y., 2019. Improved support vector regression models for predicting rock mass parameters using tunnel boring machine driving data. Tunn. Undergr. Space Technol. 91, 102958.
Liu, M.P., Sun, E., Zhang, N.N., Lai, F.W., Fuentes, R., 2024a. A new CPT virtual calibration chamber in sand based on Machine learning algorithms. J. Rock Mech. Geotech. Eng. 12, 1–15.
Liu, M.P., Sun, E., Zhang, N.N., Lai, F.W., Fuentes, R., 2024b. A virtual calibration chamber for cone penetration test based on deep-learning approaches. J. Rock. Mech. Geotech. 02 23–56.
Liu, M.P., Zhuang, P.Z., Lai, F.W., 2024c. A Bayesian optimization-genetic algorithm-based approach for automatic parameter calibration of soil models: application to clay and sand model. Comput. Geotech., 106717
Liu, H., Yue, Y.P., Liu, C., Spencer, B.F., Cui, J., 2023. Automatic recognition and localization of underground pipelines in GPR B-scans using a deep learning model. Tunn. Undergr. Space Technol. 134, 104861.
Liu, Q., Wang, X., Huang, X., Yin, X., 2020. Prediction model of rock mass class using classification and regression tree integrated AdaBoost algorithm based on TBM driving data. Tunn. Undergr. Space Technol. 106, 103595.
Liu, Z., Li, L., Fang, X., Qi, W., Shen, J., Zhou, H., Zhang, Y., 2021. Hard-rock tunnel lithology prediction with TBM construction big data using a global-attention-mechanism-based LSTM network. Autom. ConStruct. 125, 103647.
Lu, Y., Huang, M., Chen, Z., Zeng, Z., Liu, Y., Du, G., 2023. Drainage design combining drain holes and pinholes for tunnel boring machine segments subject to high water pressure. Front. Struct. Civ. Eng. 17 (11), 1723–1738.
Lu, Y., Huang, M., Zhang, C., Wang, B., Peng, L., Wei, W., 2024. Optimization of defoaming-flocculation-dewatering indices of earth pressure balance (EPB) shield muck using response surface methodology and desirability approach. J. Rock. Mech. Geotech. 1674–7755.
Pan, Y., Wu, M., Zhang, L., Chen, J., 2023. Time series clustering-enabled geological condition perception in tunnel boring machine excavation. Autom. ConStruct. 153, 104954.
Pan, Y., Zhang, L., 2022. Mitigating tunnel-induced damages using deep neural networks. Autom. ConStruct. 138, 104219.
Qian, W.F., Huang, M., Sun, C.M., Huang, B., Wang, G.F., Liu, H., 2021a. Adaptability of earth pressure balance shield tunneling in coastal complex formations: a new evaluation method. Geomech. Eng. 27 (4), 375–390.
Qian, C., Yu, W., Liu, X., Griffith, D., Golmie, N., Soc, I.C., 2021b. Towards online continuous reinforcement learning on industrial internet of things. Proc. IEEE SmartWorld-UIC/ATC/ScalCom/IoP/SCI 280–287.
Sai Madiraju, N.M., Sadat, S., Fisher, D., Karimabadi, H., 2018. Deep Temporal Clustering : Fully Unsupervised Learning of Time-Domain Features. Arxiv. 1802.
Wang, L., Pan, Q.J., Wang, S.Y., 2024. Data-driven predictions of shield attitudes using Bayesian machine learning. Comput. Geotech. 166, 106002.
Wang, Y., Zhao, J., Jiang, K., Zhou, Q., Kang, Z., Chen, C., Zhang, H., 2023. Prediction of TBM operation parameters using machine learning models based on BPSO. Adv. Eng. Inform. 56, 101955.
Wu, Z., Wei, R., Chu, Z., Liu, Q., 2021. Real-time rock mass condition prediction with TBM tunneling big data using a novel rock–machine mutual feedback perception method. J. Rock. Mech. Geotech. 13 (6), 1311–1325.
Xu, Z.W., Zhang, C., Zhou, S.H., Yang, M.H., Wu, H.A., Li, J.F., 2024. GFNS: an OpenGL-based tool for shield tunneling simulation in 3D complex stratum. Comput.

Geotech. 167, 106111.
Xu, D.M., Wang, Y.S., Huang, J.Q., Liu, S.J., Xu, S.J., Zhou, K., 2023. Prediction of geology condition for slurry pressure balanced shield tunnel with super-large diameter by machine learning algorithms. Tunn. Undergr. Space Technol. 131, 104852.
Yang, H., Wang, H., Zhou, X., 2016. Analysis on the rock–cutter interaction mechanism during the TBM tunneling process. Rock Mech. Rock Eng. 49, 1073–1090.
Yan, T., Shen, S.L., Zhou, A., 2023. GFII: a new index to identify geological features during shield tunnelling. Tunn. Undergr. Space. Technol. 142, 105440.
Yan, T., Shen, S.L., Zhou, A.N., Chen, X.S., 2022. Prediction of geological characteristics from shield operational parameters by integrating grid search and K-fold cross validation into stacking classification algorithm. J. Rock. Mech. Geotech. 14 (4), 1292–1303.
Yang, H.Q., Chu, J., Qi, X.H., Wu, S.F., Chiam, K., 2023. Bayesian evidential learning of soil-rock interface identification using boreholes. Comput. Geotech. 162, 105638.
Yin, X., Liu, Q., Huang, X., Pan, Y., 2022. Perception model of surrounding rock geological conditions based on TBM operational big data and combined unsupervised-supervised learning. Tunn. Undergr. Space Technol. 120, 104285.
Zhang, Q., Liu, Z., Tan, J., 2019. Prediction of geological conditions for a tunnel boring machine using big operational data. Autom. ConStruct. 100, 73–83.
Zhang, Z., Wang, S., Huang, X., Kwok, C.Y., 2017. TBM-block interaction during TBM tunneling in rock masses: block classification and identification. Int. J. GeoMech. 17 (5), E4016001.
Zhao, H., Ma, Q., Cao, J., Chen, Q., 2023. Dynamic neural network for incremental learning with task extended: research progress and prospect. Acta Electron. Sin. 51, 1710–1724.
Zhou, C., Xu, H., Ding, L., Wei, L., Zhou, Y., 2019a. Dynamic prediction for attitude and position in shield tunneling: a deep learning method. Autom. ConStruct. 105, 102840.
Zhou, C., Kong, T., Zhou, Y., Zhang, H., Ding, L., 2019b. Unsupervised spectral clustering for shield tunneling machine monitoring data with complex network theory. Autom. ConStruct. 107, 102924.
Zhou, X., Lu, D.C., Zhang, Y.N., Du, X.L., Rabczuk, T., 2022. An open-source unconstrained stress updating algorithm for the modified Cam-clay model. Comput. Methods Appl. Mech. Eng. 390, 114356.

**Dr Ming Huang** is currently Professor of Fuzhou University, China. He is Vice Dean of the Civil Engineering College (responsible for overall administrative work). He is a member of the Chinese Society for Rock Mechanics and Engineering. His research interests include (1) multiscale mechanical properties of bio-cemented soils and EICP/MICP-based environment-friendly ground reinforcement methods, (2) soil conditioning and muck recycling of shield tunneling, and (3) mechanical effect analysis and disaster prevention of tunnel construction in complex environments.